Received: 18 January 2018 | Revised: 15 April 2018 | Accepted: 14 May 2018

DOI: 10.1002/hbm.24227

RESEARCH ARTICLE

WILEY

Thalamic white matter in multiple sclerosis: A combined diffusion-tensor imaging and quantitative susceptibility mapping study

Niels Bergsland[1] | Ferdinand Schweser[1,2] | Michael G. Dwyer[1,2] | Bianca Weinstock-Guttman[3] | Ralph H. B. Benedict[3] | Robert Zivadinov[1,2]

[1]Buffalo Neuroimaging Analysis Center, Department of Neurology, Jacobs School of Medicine and Biomedical Sciences, University at Buffalo, State University of New York, Buffalo, New York

[2]Center for Biomedical Imaging, Clinical and Translational Science Institute, University at Buffalo, The State University of New York, Buffalo, New York

[3]Jacobs Comprehensive MS Treatment and Research Center, Department of Neurology, Jacobs School of Medicine and Biomedical Sciences, University at Buffalo, State University of New York, Buffalo, New York

Correspondence
Niels Bergsland, Buffalo Neuroimaging Analysis Center, Department of Neurology, Jacobs School of Medicine and Biomedical Sciences, State University of New York, 100 High St., Buffalo, NY 14203.
Email: npbergsland@bnac.net

Funding information
National Center for Advancing Translational Sciences of the National Institutes of Health, Grant/Award Number: UL1TR001412

Abstract

Thalamic white matter (WM) injury in multiple sclerosis (MS) remains relatively poorly understood. Combining multiple imaging modalities, sensitive to different tissue properties, may aid in further characterizing thalamic damage. Forty-five MS patients and 17 demographically-matched healthy controls (HC) were scanned with 3T MRI to obtain quantitative measures of diffusivity and magnetic susceptibility. Participants underwent cognitive evaluation with the Brief International Cognitive Assessment for Multiple Sclerosis battery. Tract-based spatial statistics identified thalamic WM. Non-parametric combination (NPC) analysis was used to perform joint inference on fractional anisotropy (FA), mean diffusivity (MD) and magnetic susceptibility measures. The association of surrounding WM lesions and thalamic WM pathology was investigated with lesion probability mapping. Compared to HCs, the greatest extent of thalamic WM damage was reflected by the combination of increased MD and decreased magnetic susceptibility (63.0% of thalamic WM, peak $p = .001$). Controlling for thalamic volume resulted in decreased FA and magnetic susceptibility (34.1%, peak $p = .004$) as showing the greatest extent. In MS patients, the most widespread association with information processing speed was found with the combination of MD and magnetic susceptibility (67.6%, peak $p = .0005$), although this was not evident after controlling for thalamic volume. For memory measures, MD alone yielded the most widespread associations (45.9%, peak $p = .012$ or 76.7%, peak $p = .001$), even after considering thalamic volume, albeit with smaller percentages. White matter lesions were related to decreased FA (peak $p = .0063$) and increased MD (peak $p = .007$), but not magnetic susceptibility, of thalamic WM. Our study highlights the complex nature of thalamic pathology in MS.

KEYWORDS
diffusion tensor imaging, MRI, multiple sclerosis, quantitative susceptibility mapping, thalamus

Abbreviations: BVMTR, Brief Visual Memory Test-Revised; CSF, cerebrospinal fluid; CVLT2, California Verbal Learning Test-2nd edition; DGM, deep gray matter; DTI, diffusion-tensor imaging; DWI, diffusion-weighted image; EDSS, Expanded Disability Status Scale; FA, fractional anisotropy; FOV, field-of-view; FSL, FMRIB's Software Library; GLM, general linear model; GM, gray matter; GRE, gradient echo; HC, healthy control; HEIDI, homogeneity enabled incremental dipole inversion; LPM, lesion probability mapping; MD, mean diffusivity; MS, multiple sclerosis; NODDI, neurite orientation dispersion and density imaging; NPC, non-parametric combination; PPMS, primary progressive multiple sclerosis; QSM, quantitative susceptibility mapping; RRMS, relapsing-remitting multiple sclerosis; SDMT, Symbol Digit Modalities Test; SPMS, secondary progressive multiple sclerosis; TBSS, tract-based spatial statistics; TE, echo time; TI, inversion time; TR, repetition time; V-SHARP, variable-kernel Sophisticated harmonic artifact reduction for phase data; WML, white matter lesion.

1 | INTRODUCTION

Multiple sclerosis (MS) is a chronic inflammatory disease affecting the central nervous system. Recently, the thalamus has received considerable attention (Minagar, et al., 2013) with studies showing that damage begins early in the disease (Bergsland et al., 2012; Quinn et al., 2014) and is associated with cognitive impairment (Benedict et al., 2013; Modica et al., 2015). Although most studies tend to treat the thalamus as a gray matter (GM) region, white matter (WM) tracts pass through it as well. In this regard, WM pathology in this structure remains relatively poorly understood, despite its potential clinical relevance, as evidenced by an association between thalamic WM microstructure

damage and cognitive status in MS (Benedict et al., 2013; Hulst et al., 2013).

Diffusion-tensor imaging (DTI) allows for the probing of tissue microstructure, which has been shown to be widely damaged in MS patients. Two commonly used DTI-derived parameters include fractional anisotropy (FA) and mean diffusivity (MD), which reflect the directional dependence and average magnitude of diffusion, respectively. WM in MS patients tends to be characterized by decreased FA and increased MD compared to healthy controls (HCs; Benedict et al., 2013; Cappellani et al., 2014) but increased thalamic FA in MS patients has also been noted (Tovar-Moll, et al., 2009). Moreover, thalamic WM MD explained additional variance in cognitive status even after accounting for structural volume (Benedict et al., 2013). The association between increased diffusivity, within much of the WM as well as within the thalamus, and cognitive decline by other reports (Hulst et al., 2013; Llufriu, et al., 2014) further highlights the utility of DTI in this regard. Although the exact causes of thalamic diffusivity alterations remain uncertain, WM lesions (WML) in connected WM fiber tracts play a role (Cappellani et al., 2014). Wallerian degeneration within the thalamus following axonal transection due to WMLs likely explains this pathological aspect. In addition, thalamic lesions are likely to have a direct impact on thalamic integrity (Minagar et al., 2013).

Iron plays a crucial role in the normal functioning of the brain due to its role in neurotransmitter production and synthesis of myelin. It has been recently suggested that thalamic iron homeostasis may be altered in MS patients (Bagnato, et al., 2011; Quinn et al., 2014; Zivadinov, et al., 2012), with some studies reporting increased thalamic iron content (Rudko, Solovey, Gati, Kremenchutzky, & Menon, 2014; Walsh et al., 2014) while others have found decreased iron levels (Schweser et al., 2018) compared to healthy individuals. Associations between thalamic iron content and cognitive impairment in MS patients have also been investigated (Fujiwara et al., 2017; Modica et al., 2015). Nevertheless, such associations specifically within the thalamic WM have yet to be investigated in MS.

Quantitative susceptibility mapping (QSM) is an imaging modality that can determine the magnetic susceptibility of tissue and is thus sensitive to the presence of iron (Hagemeier, et al., 2017; Schweser et al., 2018; Schweser, Sommer, Deistung, & Reichenbach, 2012). The technique utilizes the complex signal from a gradient echo (GRE) acquisition to derive the magnetic susceptibility distribution (Schweser, Deistung, Lehr, & Reichenbach, 2011). It remains to be determined whether altered thalamic iron dynamics have a causative role or represent an epiphenomenon of other disease processes occurring directly within the thalamus itself or following injury to connected WM tracts. While changes in WML susceptibility have been quantified using QSM (Wisnieff et al., 2015), the potential impact that WMLs themselves have on thalamic susceptibility has not yet been extensively investigated. One recent study did not detect any associations between change in susceptibility within the thalamus considered as a whole and WML volumes (Hagemeier et al., 2017). However, potential associations between thalamic WM susceptibility and lesions in the surrounding WM have not yet been reported in the literature.

Given that diffusivity and susceptibility measures relate to inherently different biological properties, we hypothesized that combining information from both modalities could further aid in characterizing MS-related thalamic WM pathology. In this regard, we utilized voxel-wise analysis techniques to compare a cohort of MS patients and healthy controls (HCs). Moreover, we explored relationships with cognitive impairment to determine whether the complementary nature of diffusion and magnetic susceptibility could better explain cognitive status than either on its own. Finally, we also investigated the association between thalamic WM tissue properties and WMLs in the surrounding tissue.

2 | MATERIALS AND METHODS

2.1 | Subjects

Sixty-two participants were included in the study, consisting of 45 MS patients (26 relapsing-remitting [RRMS], 17 secondary progressive [SPMS], 2 primary progressive [PPMS]), and 17 age- and sex-matched HCs. Participants had to be between 18 and 65 years old and were excluded if they were pregnant or in case of pre-existing medical conditions known to be associated with brain pathology (e.g., cerebrovascular disease, positive history of alcohol dependence). At the time of MRI acquisition, MS patients were relapse- and steroid-free within the last thirty days. Clinical disability in patients was quantified via the Expanded Disability Status Scale (EDSS). The 17 HC volunteers had a normal neurological examination and no history of neurologic disorders or chronic psychiatric disorders. The study was approved by the local Ethical Standards Committee at the University at Buffalo and written informed consent was obtained from all participants.

2.2 | Neuropsychological assessment

A board-certified neuropsychologist specializing in MS, and blinded to MRI findings, supervised the Brief International Cognitive Assessment for MS (BICAMS; Langdon et al., 2012), consisting of the Symbol Digit Modalities Test (SDMT; Smith, 1982; Benedict et al., 2017), California Verbal Learning Test-2nd edition (CVLT2; Delis, Kramer, Kaplan, & Ober, 2000), and the Brief Visual Memory Test-Revised (BVMTR; Benedict, 1997). Neuropsychological assessments were performed within an average of 14 days from MRI examination. Test scores were adjusted based on normative data that accounts for age and education.

2.3 | MRI acquisition

All scans were acquired on the same 3T GE Signa Excite HD 12.0 MRI scanner (General Electric, Milwaukee, WI) with an 8-channel head and neck coil. The imaging system did not undergo any major hard- or software upgrades during the study. Data for QSM were acquired using an un-accelerated 3D single-echo spoiled GRE sequence with first-order flow compensation in read and slice directions, a matrix of $512 \times 192 \times 64$ and a nominal resolution of $0.5 \times 1 \times 2$ mm^3 (field of view [FOV] = $256 \times 192 \times 128$ mm^3), flip angle = 12°, echo time (TE)/repetition time(TR) = 22/40 ms. Raw k-space data of each

channel were saved for off-line reconstruction of the images. Diffusion weighted images (DWI) were acquired with a 2D spin-echo, echo-planar imaging sequence with TE/TR = 93.1/12,500 ms, a matrix of 104 × 104 and FOV = 256 × 256 mm^2 and 57 2.5-mm thick slices without gap, for 2.5 mm isotropic resolution, 3 volumes without directional weighting (b = 0 s/mm^2), 21 unipolar diffusion gradients with b = 1,000 s/mm^2 and an acceleration factor of 2 (ASSET). An additional b = 0 s/mm^2 with reversed phase encoding was also acquired.

A T_2-weighted FLAIR was acquired with TE/inversion time (TI)/TR = 120/2,100/8,500 ms; flip angle = 90°; echo-train length = 24 with a 256 × 192 matrix (frequency × phase) and FOV = 256 × 192 mm^2 and 48 3 mm thick slices without gap, for a nominal resolution of 1 × 1 × 3 mm^3. Finally, a magnetization-prepared 3D T_1-weighted fast spoiled GRE sequence was acquired with TE/TI/TR = 2.8/900/5.9 ms, flip angle = 10°, with a 256 × 256 × 180 matrix and 1 mm isotropic resolution.

2.4 | MRI assessment

2.4.1 | Quantitative susceptibility mapping

Magnitude and phase components from the GRE acquisition were reconstructed offline using sum-of-squares and scalar phase matching (Hammond et al., 2008), respectively. Gradient non-linearity distortions were corrected (Polak, Zivadinov, & Schweser, 2015). Phase images were unwrapped with a best-path algorithm (Abdul-Rahman et al., 2007), background-field corrected with V-SHARP (Schweser et al., 2011; Wu, Li, Guidon, & Liu, 2012), and finally converted to magnetic susceptibility maps using the HEIDI algorithm (Schweser et al., 2012). Magnetic susceptibility was referenced (0 ppb) to the average susceptibility of the brain, under the assumption that a larger reference region would reduce additional inter-subject variability, compared to a smaller reference region. To investigate a potential influence of the reference region on differences between MS patients and HCs, susceptibility maps were also generated after referencing to either cerebrospinal fluid (CSF) or the internal capsule. In-house developed algorithms for QSM processing were written in MATLAB (2013b, The MathWorks, Natick, MA).

2.4.2 | Lesion assessment and tissue volumetry

WM lesions (WML) were outlined on the FLAIR image with JIM software (http://www.xinapse.com/) version 6, which utilizes a semi-automated, local thresholding technique (Zivadinov et al., 2012). Lesions confined entirely within the thalamus were also counted on the FLAIR image. Tissue volumetry was performed using the 3D T_1-weighted image, which was preprocessed using a lesion filling to reduce the impact of T1 hypointensities on segmentation quality (Gelineau-Morel et al., 2012). Specifically, SIENAX software (Smith et al., 2002) was used to obtain whole brain, total gray and total white volumes while the bilateral thalami were segmented using FIRST (Patenaude, Smith, Kennedy, & Jenkinson, 2011). Tissue volumes were normalized for head size.

2.4.3 | Diffusion-weighted imaging preprocessing

The topup tool, part of the FMRIB's Software Library (FSL) toolbox (http://www.fmrib.ox.ac.uk/fsl), was used to correct for susceptibility-based geometric distortions by calculating a field map from the pair b = 0 images with opposite phase encoding polarity (Andersson, Skare, & Ashburner, 2003). Eddy current distortions and subject movement were corrected by using the eddy tool (Andersson & Sotiropoulos, 2016), which is also part of the FSL toolbox. The diffusion tensor was then fitted and quantitative FA and MD maps were obtained.

2.4.4 | Thalamic white matter analysis

The tract-based spatial statistics (TBSS) pipeline (Smith et al., 2006) was then utilized to generate skeletonized WM maps. All subjects' FA data were aligned into a common space using nonlinear registration. WMLs were excluded from the registration cost function to minimize their impact on spatial normalization. Next, the mean FA image was thinned to create a mean FA skeleton which represents the centers of all tracts common to the group. Each subject's aligned FA and MD data were then projected onto this skeleton. QSM maps were also projected via the combination of linearly registering the GRE magnitude image to the subject's b = 0 image and the corresponding FA warp from the TBSS pipeline.

Subsequent analysis was restricted to the thalamic WM by taking the intersection of the TBSS skeleton and the Harvard-Oxford Subcortical Structural Atlas thalamic ROI. Mean FA, MD and susceptibility values within the thalamic WM skeleton were extracted. Next, joint inference on FA, MD and susceptibility maps was performed using the non-parametric combination (NPC) method (Winkler et al., 2016b) as implemented in the Permutation Analysis of Linear Models (PALM) tool (Winkler, Ridgway, Webster, Smith, & Nichols, 2014). With NPC, the joint null hypothesis of the NPC is that the null hypothesis for each of the partial tests (i.e., univariate analysis of the individual modalities) is true while the alternative is that any of them are false. It is important to note that the NPC technique does not simply take the union of any suprathreshold voxels but aggregates the results by combining the partial tests into a single joint statistic. Depending on the combining function used, non-significant partial tests can contribute to a significant joint test (Winkler et al., 2016b). As a consequence, NPC offers a more powerful alternative compared to using just a single modality or performing post-hoc analyses of multiple modalities. For example, a relatively weak effect in two different imaging modalities might not be detected when considering either on its own, but the combined statistic might reveal a significant effect. However, the addition of a modality with no signal, either on its own or after controlling for a covariate, may reduce power as a consequence of diluting the effect. Further details are provided in the Statistical analysis section.

2.4.5 | Lesion probability mapping

Lesion probability maps (LPM) were created as previously described (Bodini et al., 2011). Briefly, individual lesion masks were all put into standard MNI space and then averaged. Each voxel in the resulting image thus corresponds to the probability of corresponding to a lesion in the entire MS cohort. The PALM tool was used for non-parametric

TABLE 1 Demographic and clinical characteristics of healthy controls and multiple sclerosis patients

	HC (n = 17)	MS (n = 45)	p
Age in years, mean (*SD*)	49.1 (18.2)	57.0 (12.1)	.112
Sex, female, *N* (%)	13 (76.4)	32 (71.1)	.759
Education in years, mean (*SD*)	13.9 (2.3)	15.1 (4.0)	.323
Disease duration – mean in years (*SD*)/median (range)	–	23.4 (11.1) / 23.0 (5–43)	–
MS course – RR/SP/PP	–	26/17/2	–
EDSS – median (range)	–	3.5 (0–8)[a]	–
SDMT	55.9 (14.9)	47.0 (14.6)[b]	.037
CVLT2	55.5 (11.6)	50.6 (13.8)[b]	.198
BVMTR	24.7 (8.1)	19.9 (7.8)[b]	.037

Differences were tested using the Student's *t*-test and Fisher's exact test, as appropriate.
Abbreviations: HC = healthy controls; MS = relapsing remitting multiple sclerosis; *n* = number; SD = standard deviation; RR = relapsing-remitting; SP = secondary progressive; PP = primary progressive; EDSS = Expanded Disability Status Scale; SDMT = Symbol Digit Modalities Test; CVLT2 = California Verbal Learning Test – 2nd edition; BVMTR: Brief Visual Memory Test - Revised.
[a]EDSS was missing for four patients.
[b]Test was missing for one patient.

permutation-based inference of WML location with respect to mean FA, MD, and QSM values within the TBSS-derived thalamic WM. Further details are provided in the Statistical analysis section.

2.5 | Statistical analysis

Statistical analyses were performed using SPSS (version 21; IBM Corp., Armonk, NY). Differences in demographic characteristics between the groups were assessed using the Student's *t* test and Chi-squared, as appropriate. Comparisons between summary imaging measures were made using ANCOVA models, adjusting for age and sex.

For all voxel-wise analyses (i.e., TBSS and LPM), general linear models (GLM) were tested with PALM using tail acceleration (Winkler, Ridgway, Douaud, Nichols, & Smith, 2016a) with 500 permutations, adjusting for age and sex. Threshold-free cluster enhancement was used to identify significant clusters. For the NPC analyses, partial tests were combined using the default Fisher function, which allows for the joint statistic to be significant in the presence of partial tests in which none is significant on its own (Winkler et al., 2016b). In MS patients only, the same approach was used to assess associations between thalamic skeleton parameters and SDMT performance. To investigate the added value of the NPC approach for investigating thalamic WM, analyses were repeated after including thalamic volume as an additional covariate. Correlations between the imaging modalities were also investigated at the voxel-wise level as well as with respect to average value throughout the thalamic WM skeleton.

p Values $< .05$ were considered significant, corrected for the family-wise error rate in the case of voxel-wise analyses.

3 | RESULTS

3.1 | Demographic and clinical characteristics

Table 1 provides an overview of the demographic and clinical characteristics of the enrolled participants. HC and MS patient groups were not significantly different in terms of age and sex, but the latter performed significantly worse on the SDMT and BVMTR (both p = .037) but not the CVLT2.

3.2 | MR imaging characteristics

Table 2 provides an overview of the MR imaging comparisons between the HCs and MS patients. MS patients presented with significantly greater T2 lesion volume (p = .003) and decreased normalized whole brain (p = .008), white (p = .003), and thalamic (p = .002) volumes. Within the thalamic WM skeleton, MS patients had decreased FA (p = .022), increased MD (p = .033) and decreased susceptibility

TABLE 2 MR imaging characteristics of healthy controls and multiple sclerosis patients

	HC (n = 17)	MS (n = 45)	p
T2 lesion volume	0.9 (1.8)	15.8 (16.9)	.003
Normalized WB volume	1538.0 (110.2)	1431.7 (109.0)	.008
Normalized GM volume	775.2 (74.4)	720.3 (73.3)	.105
Normalized WM volume	762.8 (46.0)	712 (48.3)	.003
Normalized thalamic volume	19.8 (1.8)	17.2 (2.6)	.002
Thalamic WM skeleton FA	.46 (.03)	.44 (.04)	.022
Thalamic WM skeleton MD	.90 (.10)	1.08 (.27)	.033
Thalamic WM skeleton $\Delta\chi$	−1.34 (6.38)	−7.10 (6.37)	.013

Cells represent mean (standard deviation). Differences between the groups were assessed using ANCOVA models, adjusting for age and sex. Volumes are reported in milliliters. FA is a unitless measure. MD is reported in in $mm^2/s \times 10^{-3}$. Susceptibility is reported in ppb.
Abbreviations: HC = healthy controls; MS = relapsing remitting multiple sclerosis; *n* = number; WB = whole brain; GM = gray matter; WM = white matter; FA = fractional anisotropy; MD = mean diffusivity; $\Delta\chi$ = magnetic susceptibility.

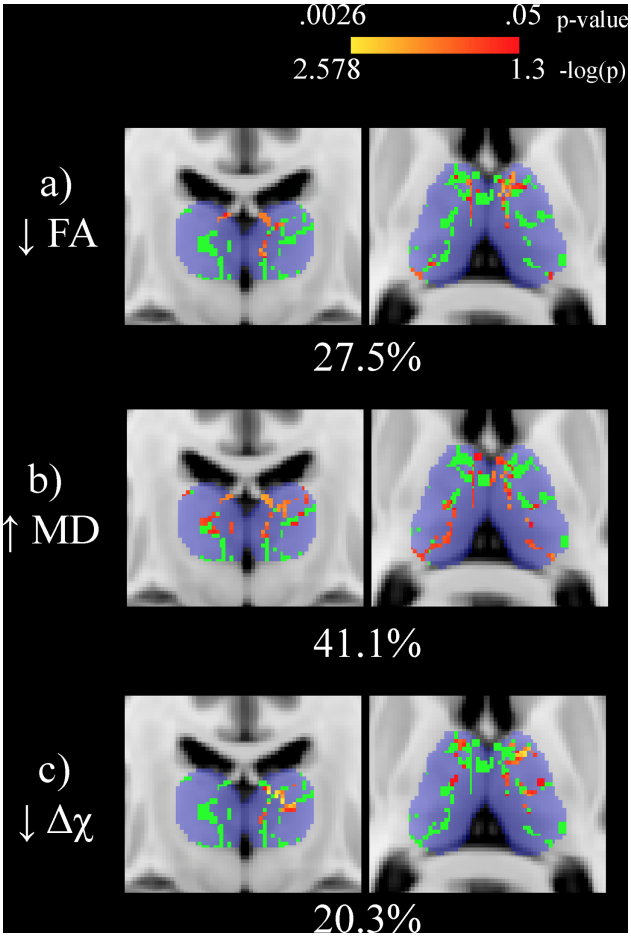

FIGURE 1 Univariate voxel-wise analysis of the thalamic white matter skeleton (shown in green) comparing healthy controls (HCs) and multiple sclerosis (MS) patients. Significant differences ($p < .05$) are shown in red-yellow with p values having been log transformed for improved visibility. Warmer colors are indicative of smaller p values. Decreased fractional anisotropy, increased mean diffusivity, and decreased susceptibility are seen in MS patients compared to HCs. Percentages refer to the proportion of significantly different voxels between MS patients and HCs in the thalamic skeleton. The Harvard-Oxford thalamic ROI is shown for reference in transparent blue. The slice shown corresponds to standard space MNI coordinates of $Y = -17$, $Z = 8$.
Abbreviations: FA: fractional anisotropy; MD = mean diffusivity; $\Delta\chi$ = magnetic susceptibility; HC = healthy control; MS = multiple sclerosis [Color figure can be viewed at wileyonlinelibrary.com]

($p = .013$). For most participants, thalamic lesions were not seen: 11 patients had one, 1 patient had two, and 2 patients had three.

3.3 | Voxel-wise group differences within the thalamic WM skeleton

Results from the univariate analyses are shown in Figure 1. With respect to HCs, the thalamic WM skeleton was significantly different in MS patients in terms of decreased FA (27.5%, peak $p = .005$; panel a), increased MD (41.1%, peak $p = .0061$; panel b) and decreased susceptibility (20.3%, peak $p = .0026$; panel c). None of the opposite contrasts in the GLMs revealed any significant differences. Results from the NPC analyses are shown in Figure 2. When combining multiple modalities, significantly different voxels in the thalamic WM skeleton were as follows: decreased FA and increased MD (45.4%, peak $p = .0028$; panel a), decreased FA and decreased susceptibility (48.5%, peak $p = .0006$; panel b), increased MD and decreased susceptibility (63.0%, peak $p = .0010$; panel c) and decreased FA, increased MD, and decreased susceptibility (60.5%, peak $p = .0009$; panel d). When controlling for thalamic volume, MS patients were significantly different only in terms

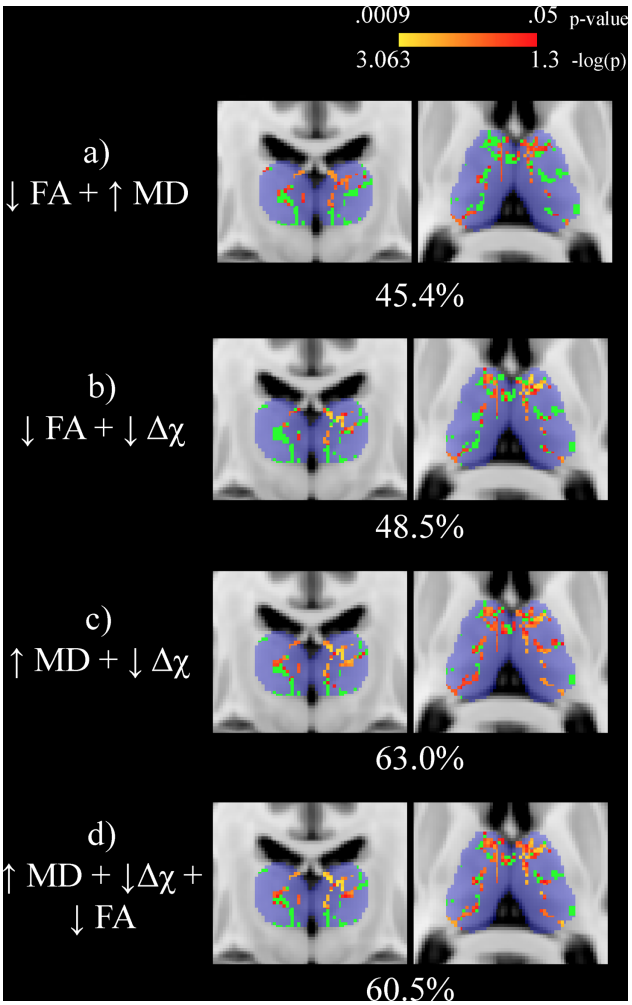

FIGURE 2 Nonparametric combination voxel-wise analysis of the thalamic white matter skeleton (shown in green) between healthy controls (HCs) and multiple sclerosis (MS) patients. Significant differences ($p < .05$) are shown in red-yellow with p-values having been log transformed for improved visibility. Warmer colors are indicative of smaller p values. Percentages refer to the proportion of significantly different voxels between MS patients and HCs in the thalamic skeleton. In each combination, decreased fractional anisotropy, increased mean diffusivity, and decreased magnetic susceptibility are seen in MS patients compared to HCs. The Harvard-Oxford thalamic ROI is shown for reference in transparent blue. The slices shown corresponds to standard space MNI coordinates of $Y = -17$, $Z = 8$.
Abbreviations: FA = fractional anisotropy; MD = mean diffusivity; $\Delta\chi$ = magnetic susceptibility; HC = healthy control; MS = multiple sclerosis [Color figure can be viewed at wileyonlinelibrary.com]

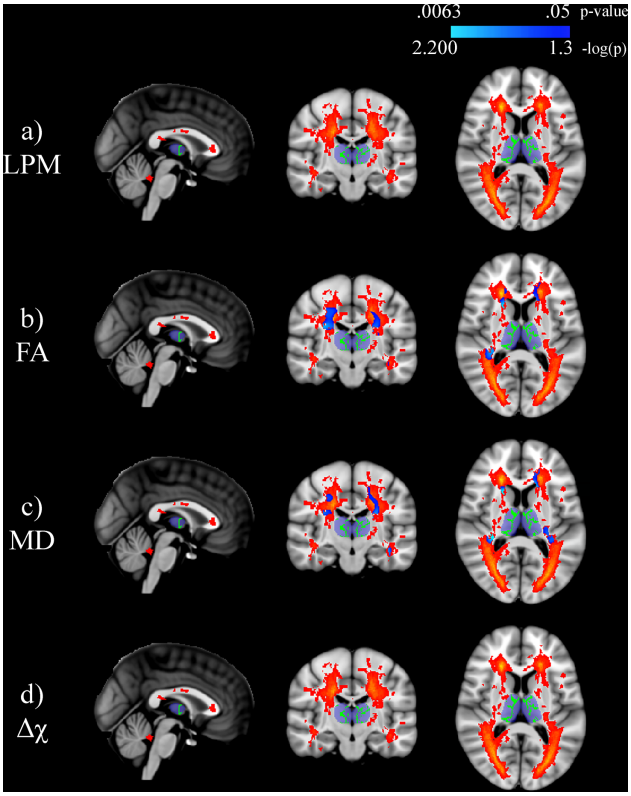

FIGURE 3 Lesion probability mapping (LPM) of multiple sclerosis (MS) patients relating white matter (WM) lesion location to mean thalamic WM skeleton (shown in green) parameters. The top panel shows the LPM image with warmer colors corresponding to increased probability of a lesional voxel in the MS cohort. Significant associations ($p < .05$) are shown in blue to light blue with p-values having been log transformed for improved visibility. The Harvard-Oxford thalamic ROI is shown for reference in transparent blue. Note that there are no significant associations with lesion location and mean susceptibility of the thalamic WM skeleton. The slice shown corresponds to standard space MNI coordinates of $X = 0, Y = -17, Z = 8$.
Abbreviations: FA = fractional anisotropy; MD = mean diffusivity; $\Delta\chi$ = magnetic susceptibility; LPM = lesion probability mapping; WM = white matter; MS = multiple sclerosis [Color figure can be viewed at wileyonlinelibrary.com]

of decreased thalamic WM susceptibility (21.6%, peak $p = .004$) in the univariate analyses. In the combined analysis, the results were as follows: decreased FA and increased MD (0.1%, peak $p = .049$); decreased FA and decreased susceptibility (28.1%, peak $p = .002$); increased MD and decreased susceptibility (25.5%, peak $p = .005$) and decreased FA, increased MD and decreased susceptibility (34.1%, peak $p = .004$). Analyses were repeated after restricting the MS group to 28 patients that were more closely matched in terms of age (mean difference of 1.6 years, $p = .739$). The results were not substantially different compared to the original analyses (results not shown).

3.4 | Correlation between FA, MD, and susceptibility within the thalamic WM skeleton

As expected, FA and MD were inversely correlated in nearly all of the thalamic WM skeleton (96.6%, peak $p = .002$). Magnetic susceptibility was positively correlated with FA in a small number of voxels (6.9%, peak $p = .0004$) while an inverse relationship was found in even fewer areas (0.7%, minimum $p = .0019$). Finally, MD and susceptibility were positively correlated in a limited number of voxels (0.8%, peak $p = .0134$) while being inversely correlated to a greater, although still limited, extent (17.8%, peak $p = .0003$). When considering the mean value throughout the entire thalamic WM skeleton, only FA and MD were related ($r = -.760$, $p < .00001$); susceptibility did not correlate with either of the DTI metrics. There were no significant interactions with group membership for any of the correlations.

3.5 | Lesion probability mapping

LPM results are shown in Figure 3. The LPM analysis revealed a WML distribution typical of MS, within increased likelihood in the periventricular region (panel a). Lesion probability was highest (62.2%) at MNI standard coordinate: $X = 21$, $Y = 32$, $Z = 2$. WMLs were associated with decreased FA (peak $p = .0063$; panel b) and increased MD (peak $p = .0070$; panel c) within the thalamic WM skeleton. The opposite contrasts did not reveal any significant relationships nor were there any associations in either direction with respect to average susceptibility of thalamic WM skeleton (panel d).

3.6 | Voxel-wise associations with neuropsychological outcomes

Voxel-wise associations between thalamic WM measures and neuropsychological outcomes in MS patients are summarized in Table 3. Univariate associations are shown in Figure 4 while results from the NPC analysis are presented in Figure 5. In terms of SDMT performance, the largest proportion of significantly associated voxels was found using the combination of MD and magnetic susceptibility modalities. However, controlling for thalamic volume resulted in all analyses failing to reach significance. On the other hand, for BVMTR and CVLT2 outcomes, univariate analysis with MD yielded the largest proportion of significant voxels in the thalamic WM skeleton. The same was true when controlling for thalamic volume.

3.7 | Influence of reference region on group MS versus HC group differences

Average susceptibility of the thalamic skeleton was reduced, but not significantly so, in MS patients when using either CSF ($p = .091$) or the internal capsule ($p = .152$) as the reference region. However, voxel-wise analyses were very similar to those obtained when referencing to the average susceptibility of the brain. Results are presented in terms of referencing either CSF or the internal capsule. Specifically, in univariate analyses, MS patients presented with decreased susceptibility in 13.0% (peak $p = .0010$) or 12.1% (peak $p = .0009$). Combining with FA, 45.4% (peak $p = .0002$) or 43.5% (peak $p = .00002$) of the thalamic WM skeleton was significantly different in MS patients. Combining with MD yielded either 61.7% (peak $p = .0002$) or 56.5% (peak $p = .0002$). Finally, when combining all FA, MD and susceptibility resulted in either 59.6% (peak $p = .0002$) or 57.2% (peak $p = .0002$).

TABLE 3 Voxel-wise associations between the thalamic WM skeleton and neuropsychological outcomes

	Univariate analyses			Non-parametric combination analyses			
	FA	MD	$\Delta\chi$	FA + MD	FA+$\Delta\chi$	MD+$\Delta\chi$	FA+ MD+$\Delta\chi$
SDMT	31.8 (.001)	57.0 (.002)	3.6 (.009)	43.9 (.001)	39.7 (.0005)	67.6 (.0005)	65.3 (.0005)
BVMTR	35.5 (.001)	76.7 (.001)	0 (.06)	62.7 (.001)	40.5 (.0005)	76.0 (.0004)	72.7 (.002)
CVLT2	0 (.071)	45.9 (.012)	0 (.286)	14.4 (.02)	0 (.14)	38.6 (.022)	10.0 (.023)
	Controlling for thalamic volume						
SDMT	0 (.418)	0 (.108)	0 (.576)	0 (.218)	0 (0.272)	0 (.099)	0 (.150)
BVMTR	0.4 (.035)	46.1 (.013)	0 (.448)	28.7 (.014)	0.8 (.034)	44.3 (.003)	29.0 (.005)
CVLT2	0 (.106)	23.6 (.014)	0 (.312)	7.3 (.028)	0 (.184)	13.3 (.033)	2.3 (.035)

Cells represent percentage of significant voxels (peak *p* value).
Abbreviations: SDMT = Symbol Digit Modalities Test; CVLT2 = California Verbal Learning Test - 2nd edition; BVMTR: Brief Visual Memory Test – Revised; FA = fractional anisotropy; MD = mean diffusivity; $\Delta\chi$ = magnetic susceptibility.

4 | DISCUSSION

In this study, we combined quantitative diffusivity and magnetic susceptibility measures in an attempt to better characterize the extent of thalamic WM damage in MS with respect to HCs as well its relation to cognition. Our findings highlight the complex nature of thalamic pathology in MS.

In the univariate analyses, voxel-wise differences within the thalamic WM skeleton between HCs and MS patients were greatest for MD followed by FA and susceptibility measures. Compared to MD alone though, the addition of FA yielded only a marginal improvement, as might be expected given that they are highly correlated metrics. On the other hand, a larger portion of the thalamic skeleton was found to be significantly affected when including susceptibility measures in the

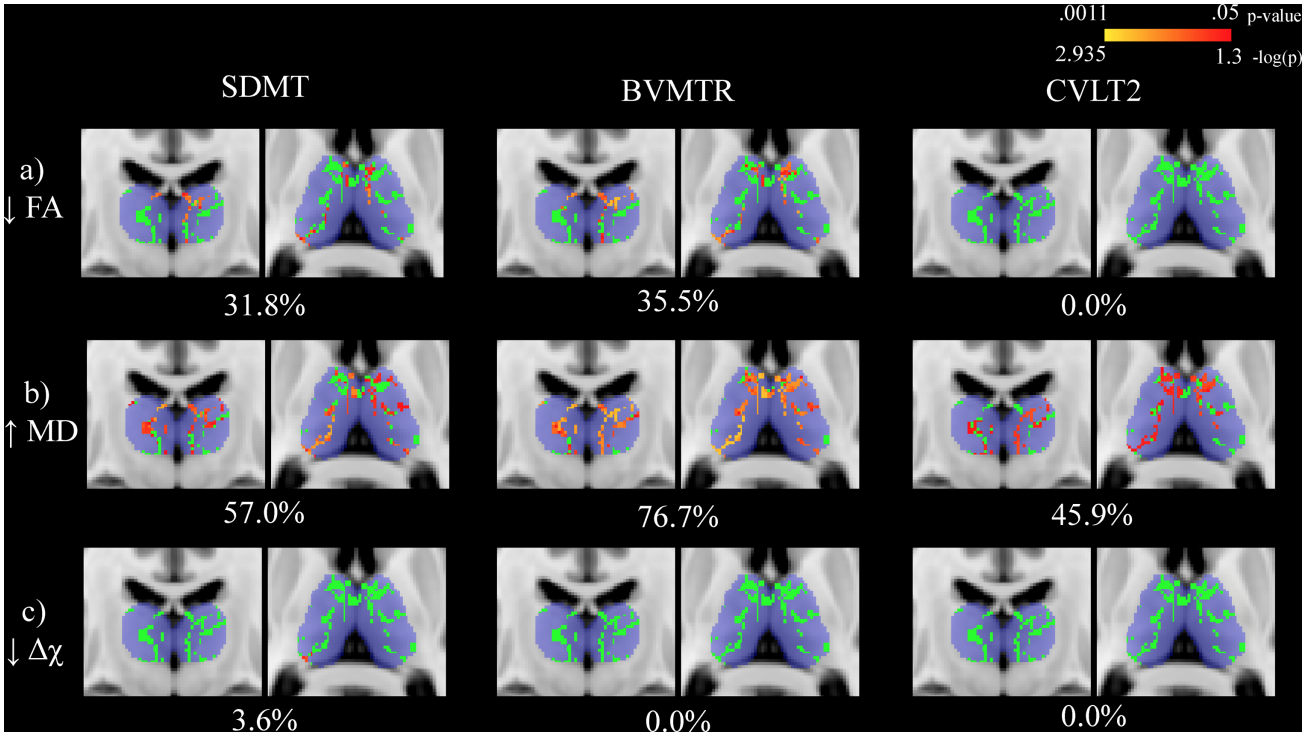

FIGURE 4 Univariate voxel-wise analysis assessing the relationship between cognitive assessment performance and thalamic white matter (WM) metrics in multiple sclerosis (MS) patients. The thalamic WM skeleton is shown in green overlaid on top of the Harvard-Oxford thalamic ROI in blue. Significant associations ($p < .05$) are shown in red-yellow with *p* values having been log transformed for improved visibility. Warmer colors are indicative of smaller *p* values. Decreased fractional anisotropy, increased mean diffusivity, and decreased susceptibility were related to decreased performance. Percentages refer to the proportion of significantly associated voxels with performance. The slices shown corresponds to standard space MNI coordinates of $Y = -17$, $Z = 8$.
Abbreviations: SDMT = Symbol Digit Modalities Test; BVMTR = Brief Visual Memory Test – Revised; CVLT2 = California Verbal Learning Test - 2nd edition; FA = fractional anisotropy; MD = mean diffusivity; $\Delta\chi$ = magnetic susceptibility [Color figure can be viewed at wileyonlinelibrary.com]

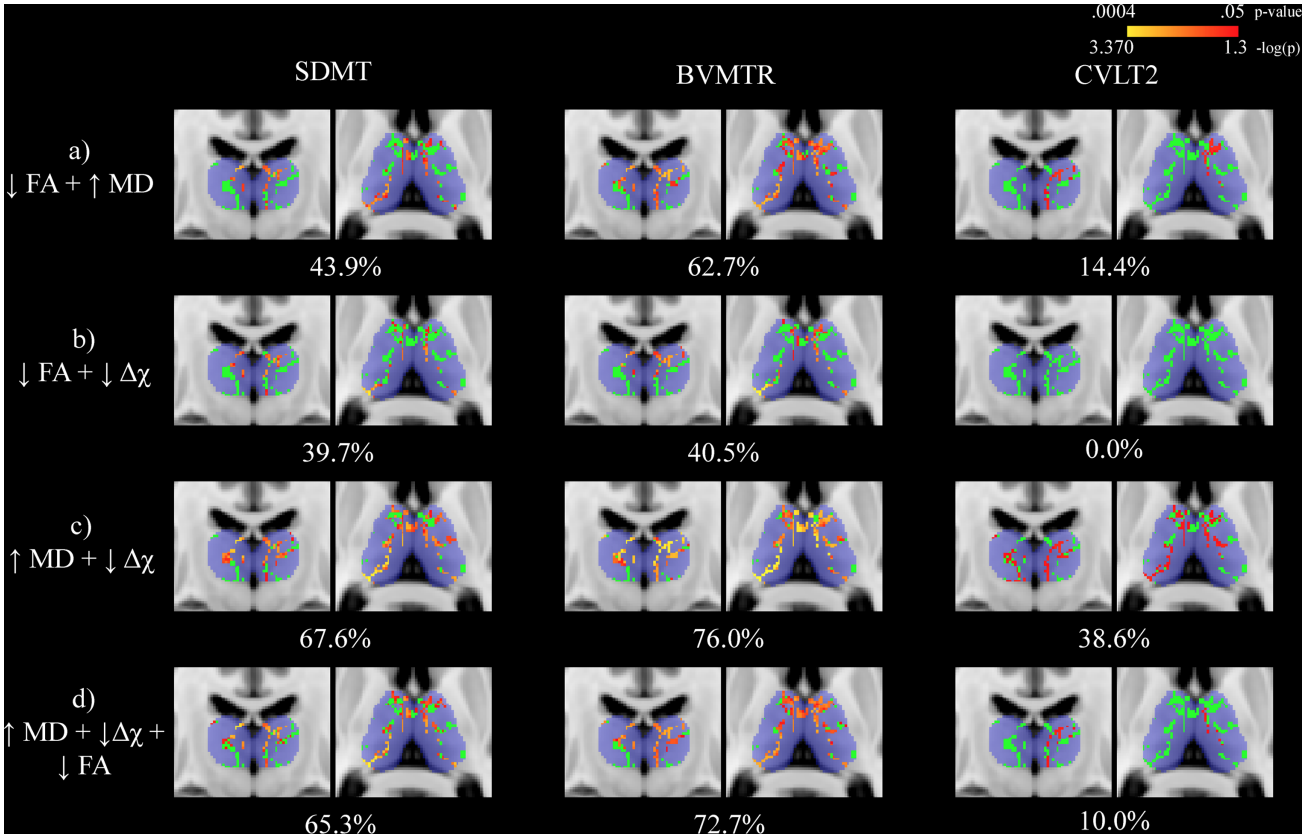

FIGURE 5 Nonparametric combination voxel-wise analysis assessing the relationship between cognitive assessment performance and thalamic white matter (WM) metrics in multiple sclerosis (MS) patients. The thalamic WM skeleton is shown in green overlaid onto of the Harvard-Oxford thalamic ROI in blue. Significant differences ($p < .05$) are shown in red-yellow with *p*-values having been log transformed for improved visibility. Warmer colors are indicative of smaller *p*-values. Percentages refer to the proportion of voxels significantly associated with performance. The slices shown corresponds to standard space MNI coordinates of $Y = -17$, $Z = 8$.
Abbreviations: SDMT = Symbol Digit Modalities Test; BVMTR = Brief Visual Memory Test – Revised; CVLT2 = California Verbal Learning Test - 2nd edition; FA = fractional anisotropy; MD = mean diffusivity; $\Delta\chi$ = magnetic susceptibility; HC = healthy control [Color figure can be viewed at wileyonlinelibrary.com]

combined analysis, compared to MD alone. As MD and susceptibility values were correlated in less than 20% of the thalamic WM skeleton, our findings highlight the complementary nature of diffusion and susceptibility measures. The combined approach allowed for the detection of more widespread MS-related damage compared to HCs than could be evidenced using only a single modality. Interestingly, while the proportion of significantly different voxels in the thalamic WM skeleton was the smallest for magnetic susceptibility, only this modality revealed significant associations when controlling for thalamic volume in the univariate analyses. However, in the combined analysis, the addition of diffusion modalities resulted in the detection of more widespread damage than magnetic susceptibility alone. Taken together, our findings support the notion of multiple pathogenetic mechanisms simultaneously affecting thalamic WM in MS (Louapre et al., 2017), which can apparently be captured using a multimodal approach as in the current work.

On the one hand, our DTI findings further confirm the results from previous studies showing altered thalamic WM integrity in MS patients (Benedict et al., 2013; Hulst et al., 2013). On the other hand, the current study is one of the first to investigate thalamic WM susceptibility. Susceptibility of the thalamus as a whole has been an active area of research with discrepant reports due to a number of factors, such as patient characteristics (Quinn et al., 2014) or region of interest definitions (Quinn et al., 2014; Zivadinov et al., 2012). For example, a recent voxel-wise study utilizing 7T MRI reported increased overall thalamic susceptibility in MS patients compared to HCs, which was also positively associated with EDSS scores (Rudko et al., 2014). Thalamic WM was not specifically investigated though and the cohort consisted of patients only in the earlier phases of the disease with 4 patients with clinically isolated syndrome and 21 with RRMS. Moreover, the patients in that study were considerably younger with a mean age of 37.3 years compared to 57.0 years in the current study. Given the known nonlinear nature of thalamic iron changes in HCs, with increases in the first several decades of life followed by subsequent reductions beginning around mid-life (Hallgren & Sourander, 1958), our findings are not necessarily contradictory. Instead, they may simply reflect different snapshots in the temporal evolution of thalamic iron dynamics in MS (Louapre et al., 2017). A comprehensive overview of studies investigating thalamic susceptibility in MS was recently published (Schweser et al., 2018). That study also found lower magnetic susceptibility in a

cohort 40 RRMS and 40 SPMS patients compared to HCs, in line with the present findings. It should be mentioned that our results do not appear to be related to the reference region used during generation of the susceptibility maps; the voxel-wise results were generally very similar when referencing to either CSF or the internal capsule rather than the average of the brain.

The results from the LPM analysis confirmed the previously reported association between WMLs and increased microstructural damage, as assessed by DTI, of the subcortical structures (Cappellani et al., 2014). While the exact mechanisms are not fully understood, anterograde and retrograde degeneration secondary to axonal transection are thought to play key roles (Kipp et al., 2015). Indeed, WMLs were significantly associated with decreased FA and increased MD values within the thalamic WM skeleton. Interestingly though, WML presence was not related to the average susceptibility. These results suggest that decreased thalamic WM susceptibility stems from a pathological process that is at least partially independent from focal damage in the surrounding WM. It seems plausible that thalamic lesions play a role as well. We were unable to investigate this hypothesis though as we detected a limited number of thalamic lesions. However, it must be mentioned that we almost certainly failed to detect a considerable proportion of them in our cohort, as imaging at higher field strengths has revealed a much greater prevalence (Harrison et al., 2015).

Furthermore, our results confirm the association between thalamic WM damage and cognitive impairment in MS as previously reported (Benedict et al., 2013; Hulst et al., 2013). Diffusivity changes were indeed consistently associated with information processing speed, as measured by the SDMT, and memory, as quantified by BVMTR (visual memory) and CVLT2 (verbaml memory). However, magnetic susceptibility was related only to SDMT performance. Moreover, the combined analysis including diffusivity measures and magnetic susceptibility revealed a more widespread association for SDMT but a more restricted spatial pattern compared to MD alone for BVMTR and CVLT2 outcomes. These results are unlike those from the group comparison with HCs where the combination of diffusivity and magnetic susceptibility modalities revealed a more widespread involvement of thalamic damage than either on its own. The exact interpretation of these apparent discrepancies is unclear at this time and warrant further investigation. In addition, portions of the thalamic WM skeleton remained significantly associated with BVMTR and CVLT2, even after controlling for thalamic volume, which are for the most part in line with previous work except for the lack of association with SDMT (Benedict et al., 2013). The lack of a relationship with magnetic susceptibility is supported by two previous studies that showed iron levels did not explain additional variance in cognitive outcomes after controlling for thalamic volume (Fujiwara et al., 2017; Modica et al., 2015). Overall, our findings point towards thalamic WM iron as having a weaker role in explaining cognitive status compared to that of diffusivity changes, especially when also considering structural atrophy.

Our study is not without limitations. First, its cross-sectional nature prevents us from drawing conclusions regarding the temporal relationships of the mechanisms involved in intrathalamic damage. Second, the identification of thalamic WM was based on the results of the TBSS pipeline. While this approach overcomes some of the difficulty inherent in aligning WM tracts, it has not been validated to accurately separate thalamic WM from the surrounding GM. Moreover, the diffusion acquisition had relatively coarse spatial and angular resolutions, which may have resulted in a certain degree of partial voluming from the surrounding GM. Although the medullary laminae were evident in the thalamic WM skeleton, some caution is thus warranted in the interpretation of our results. While the impact of WM fiber orientation on susceptibility measures is not yet fully understood, a recent study found that voxels with a FA values less than 0.6 can be reliably measured (Lancione, Tosetti, Donatelli, Cosottini, & Costagli, 2017). In the current study, an average of 2.6% $\pm$ 2.9% of the skeleton was greater than this threshold. If the challenges associated with investigating susceptibility in the WM are eventually resolved, future studies may be warranted to extend our findings to the whole brain. Third, we only investigated DTI-derived FA and MD diffusion parameters. On the other hand, more advanced modeling techniques can provide measures that are potentially more informative. For example, NODDI (Zhang, Schneider, Wheeler-Kingshott, & Alexander, 2012) provides neurite density and orientation dispersion estimates, which are more biologically specific with regards to the underlying tissue properties. Fourth, there are well-known effects of age on both diffusion properties (Westlye et al., 2010) and magnetic susceptibility (Keuken et al., 2017; Zhang et al., 2013). We controlled for age in our statistical modeling and also repeated our analyses after restricting the MS cohort to a cohort that was better matched in terms of age. Thus, age is unlikely to be a key driver of our results. Nonetheless, our results should be confirmed in future studies, especially since our HC group was relatively small. Fifth, given the relatively small sample size, we did not investigate whether there were differences between the different MS phenotypes. Finally, investigations with phantom and in vivo data have suggested that iron can influence DTI measurements as a result of a decreased signal to noise ratio, (Rulseh, Keller, Tintěra, Kožíšek, & Vymazal, 2013; Zhang et al., 2013) or cross-term effects with the diffusion gradients (Fujiwara, Uhrig, Amadon, Jarraya, & Le Bihan, 2014), resulting in artificially lowered MD and increased FA values. As a consequence, greater iron content in HCs may result in an overestimation of diffusivity differences between the HC and MS groups. Similarly, the strength of the FA and MD associations with neuropsychological outcomes in the MS cohort may potentially be underestimated in areas of thalamic WM that have relatively more iron.

In conclusion, combining quantitative measures of diffusion and susceptibility can provide additional insight into MS-related tissue damage compared to using a single modality on its own. Longitudinal studies using the same imaging techniques may help to better understand the temporal evolution of thalamic WM damage.

ACKNOWLEDGMENTS

The authors gratefully acknowledge all the study volunteers as well as the developers of the FSL software packages. The content is solely the responsibility of the authors and does not necessarily represent the official views of the NIH.

DISCLOSURES

N. Bergsland has nothing to disclose. F. Schweser has received personal compensation from Toshiba Canada Medical Systems Limited and Goodwin Procter LLP for speaking and consultant fees. He received financial support for research activities from SynchroPET Inc. and travel sponsorship from GE Healthcare and SynchroPET Inc. MG Dwyer has received consultant fees from Claret Medical and EMD Serono and research grant support from Novartis. B. Weinstock-Guttman has received honoraria as a speaker and as a consultant for Biogen Idec, Teva Pharmaceuticals, EMD Serono, Genzyme, Sanofi, Novartis, and Acorda. Dr. Weinstock-Guttman received research funds from Biogen Idec, Teva Pharmaceuticals, EMD Serono, Genzyme, Sanofi, Novartis, Acorda. R HB Benedict has received research support from Accorda, Novartis, Genzyme, Biogen, and Mallinckrodt Pharmaceuticals, is on the speakers' bureau for EMD Serono (designing CME courses), consults for Biogen, Genentech, Genzyme and Novartis, and receives royalties from Psychological Assessment Resources. R. Zivadinov has received personal compensation from EMD Serono, Genzyme-Sanofi, Novartis, Claret-Medical, Celgene for speaking and consultant fees. He received financial support for research activities from Claret Medical, Genzyme-Sanofi, QuintilesIMS Health, Novartis and Intekrin-Coherus. None of the above potential conflicts of interest are related to the current work.

ORCID

Niels Bergsland http://orcid.org/0000-0002-7792-0433

REFERENCES

Abdul-Rahman, H. S., Gdeisat, M. A., Burton, D. R., Lalor, M. J., Lilley, F., & Moore, C. J. (2007). Fast and robust three-dimensional best path phase unwrapping algorithm. *Applied Optics*, *46*(26), 6623–6635.

Andersson, J. L., Skare, S., & Ashburner, J. (2003). How to correct susceptibility distortions in spin-echo echo-planar images: Application to diffusion tensor imaging. *NeuroImage*, *20*(2), 870–888.

Andersson, J. L. R., & Sotiropoulos, S. N. (2016). An integrated approach to correction for off-resonance effects and subject movement in diffusion MR imaging. *NeuroImage*, *125*, 1063–1078.

Bagnato, F., Hametner, S., Yao, B., van Gelderen, P., Merkle, H., Cantor, F. K., … Duyn, J. H. (2011). Tracking iron in multiple sclerosis: A combined imaging and histopathological study at 7 Tesla. *Brain*, *134*(12), 3602–3615.

Benedict, R. H. B. (1997). *Brief Visuospatial Memory Test - Revised: Professional Manual*. Odessa, Florida: Psychological Assessment Resources, Inc.

Benedict, R. H., DeLuca, J., Phillips, G., LaRocca, N., Hudson, L. D., & Rudick, R. (2017). Multiple sclerosis outcome assessments C: Validity of the symbol digit modalities test as a cognition performance outcome measure for multiple sclerosis. *Mult Scler*, *23*(5), 721–733.

Benedict, R. H., Hulst, H. E., Bergsland, N., Schoonheim, M. M., Dwyer, M. G., Weinstock-Guttman, B., … Zivadinov, R. (2013). Clinical significance of atrophy and white matter mean diffusivity within the thalamus of multiple sclerosis patients. *Multiple Sclerosis Journal*, *19*(11), 1478–1484.

Bergsland, N., Horakova, D., Dwyer, M. G., Dolezal, O., Seidl, Z. K., Vaneckova, M., … Zivadinov, R. (2012). Subcortical and cortical gray matter atrophy in a large sample of patients with clinically isolated syndrome and early relapsing-remitting multiple sclerosis. *American Journal of Neuroradiology*, *33*(8), 1573–1578.

Bodini, B., Battaglini, M., De Stefano, N., Khaleeli, Z., Barkhof, F., Chard, D., … Ciccarelli, O. (2011). T2 lesion location really matters: A 10 year follow-up study in primary progressive multiple sclerosis. *Journal of Neurology, Neurosurgery, and Psychiatry*, *82*(1), 72–77.

Cappellani, R., Bergsland, N., Weinstock-Guttman, B., Kennedy, C., Carl, E., Ramasamy, D. P., … Zivadinov, R. (2014). Subcortical deep gray matter pathology in patients with multiple sclerosis is associated with white matter lesion burden and atrophy but not with cortical atrophy: A diffusion tensor MRI study. *AJNR. American Journal of Neuroradiology*, *35*(5), 912–919.

Delis, D. C., Kramer, J. H., Kaplan, E., & Ober, B. A. (2000). *Califorina Verbal Learning Test - Second Edition*. San Antonio, TX: The Psychological Corporation.

Fujiwara, E., Kmech, J. A., Cobzas, D., Sun, H., Seres, P., Blevins, G., & Wilman, A. H. (2017). Cognitive implications of deep gray matter iron in multiple sclerosis. *American Journal of Neuroradiology*, *38*(5), 942–948.

Fujiwara, S., Uhrig, L., Amadon, A., Jarraya, B., & Le Bihan, D. (2014). Quantification of iron in the non-human primate brain with diffusion-weighted magnetic resonance imaging. *NeuroImage*, *102*, 789–797.

Gelineau-Morel, R., Tomassini, V., Jenkinson, M., Johansen-Berg, H., Matthews, P. M., & Palace, J. (2012). The effect of hypointense white matter lesions on automated gray matter segmentation in multiple sclerosis. *Human Brain Mapping*, *33*(12), 2802–2814.

Hagemeier, J., Zivadinov, R., Dwyer, M. G., Polak, P., Bergsland, N., Weinstock-Guttman, B., … Schweser, F. (2017). *NeuroImage: Clinical*, Changes of deep gray matter magnetic susceptibility over 2 years in multiple sclerosis and healthy control brain. In press.

Hallgren, B., & Sourander, P. (1958). The effect of age on the non-haemin iron in the human brain. *Journal of Neurochemistry*, *3*(1), 41–51.

Hammond, K. E., Lupo, J. M., Xu, D., Metcalf, M., Kelley, D. A., Pelletier, D., … Nelson, S. J. (2008). Development of a robust method for generating 7.0 T multichannel phase images of the brain with application to normal volunteers and patients with neurological diseases. *NeuroImage*, *39*(4), 1682–1692.

Harrison, D. M., Oh, J., Roy, S., Wood, E. T., Whetstone, A., Seigo, M. A., … Calabresi, P. A. (2015). Thalamic lesions in multiple sclerosis by 7T MRI: Clinical implications and relationship to cortical pathology. *Multiple Sclerosis Journal*, *21*(9), 1139–1150.

Hulst, H. E., Steenwijk, M. D., Versteeg, A., Pouwels, P. J., Vrenken, H., Uitdehaag, B. M., … Barkhof, F. (2013). Cognitive impairment in MS: Impact of white matter integrity, gray matter volume, and lesions. *Neurology*, *80*(11), 1025–1032.

Keuken, M. C., Bazin, P. L., Backhouse, K., Beekhuizen, S., Himmer, L., Kandola, A., … Forstmann, B. U. (2017). Effects of aging on T(1), T(2)*, and QSM MRI values in the subcortex. *Brain Structure and Function*, *222*(6), 2487–2505.

Kipp, M., Wagenknecht, N., Beyer, C., Samer, S., Wuerfel, J., & Nikoubashman, O. (2015). Thalamus pathology in multiple sclerosis: From biology to clinical application. *Cellular and Molecular Life Sciences*, *72*(6), 1127–1147.

Lancione, M., Tosetti, M., Donatelli, G., Cosottini, M., & Costagli, M. (2017). The impact of white matter fiber orientation in single-acquisition quantitative susceptibility mapping. *NMR in Biomedicine*, *30*(11), https://doi.org/10.1002/nbm.3798. Epub 2017 Sep 13.

Langdon, D. W., Amato, M. P., Boringa, J., Brochet, B., Foley, F., Fredrikson, S., … Benedict, R. H. (2012). Recommendations for a brief international cognitive assessment for multiple sclerosis (BICAMS). *Multiple Sclerosis Journal*, *18*(6), 891–898.

Llufriu, S., Martinez-Heras, E., Fortea, J., Blanco, Y., Berenguer, J., Gabilondo, I., ... Saiz, A. (2014). Cognitive functions in multiple sclerosis: Impact of gray matter integrity. *Multiple Sclerosis Journal*, *20*(4), 424–432.

Louapre, C., Govindarajan, S. T., Gianni, C., Madigan, N., Sloane, J. A., Treaba, C. A., ... Mainero, C. (2017). Heterogeneous pathological processes account for thalamic degeneration in multiple sclerosis: Insights from 7 T imaging. *Multiple Sclerosis Journal*, 135245851772638. 1352458517726382.

Minagar, A., Barnett, M. H., Benedict, R. H., Pelletier, D., Pirko, I., Sahraian, M. A., ... Zivadinov, R. (2013). The thalamus and multiple sclerosis: Modern views on pathologic, imaging, and clinical aspects. *Neurology*, *80*(2), 210–219.

Modica, C. M., Zivadinov, R., Dwyer, M. G., Bergsland, N., Weeks, A. R., & Benedict, R. H. (2015). Iron and volume in the deep gray matter: Association with cognitive impairment in multiple sclerosis. *AJNR. American Journal of Neuroradiology*, *36*(1), 57–62.

Patenaude, B., Smith, S. M., Kennedy, D. N., & Jenkinson, M. (2011). A Bayesian model of shape and appearance for subcortical brain segmentation. *NeuroImage*, *56*(3), 907–922.

Polak, P., Zivadinov, R., & Schweser, F. (2015). Gradient unwarping for phase imaging reconstruction. *Proceedings of the International Society for Magnetic Resonance in Medicine*, *2015*, p3736.

Quinn, M. P., Gati, J. S., Klassen, M. L., Lee, D. H., Kremenchutzky, M., & Menon, R. S. (2014). Increased deep gray matter iron is present in clinically isolated syndromes. *Multiple Sclerosis and Related Disorders*, *3*(2), 194–202.

Rudko, D. A., Solovey, I., Gati, J. S., Kremenchutzky, M., & Menon, R. S. (2014). Multiple sclerosis: Improved identification of disease-relevant changes in gray and white matter by using susceptibility-based MR imaging. *Radiology*, *272*(3), 851–864.

Rulseh, A. M., Keller, J., Tintěra, J., Kožíšek, M., & Vymazal, J. (2013). Chasing shadows: What determines DTI metrics in gray matter regions? An in vitro and in vivo study. *Journal of Magnetic Resonance Imaging*, *38*(5), 1103–1110.

Schweser, F., Deistung, A., Lehr, B. W., & Reichenbach, J. R. (2011). Quantitative imaging of intrinsic magnetic tissue properties using MRI signal phase: An approach to in vivo brain iron metabolism? *NeuroImage*, *54*(4), 2789–2807.

Schweser, F., Raffaini Duarte Martins, A. L., Hagemeier, J., Lin, F., Hanspach, J., Weinstock-Guttman, B., ... Zivadinov, R. (2018). Mapping of thalamic magnetic susceptibility in multiple sclerosis indicates decreasing iron with disease duration: A proposed mechanistic relationship between inflammation and oligodendrocyte vitality. *NeuroImage*, *167*, 438–452.

Schweser, F., Sommer, K., Deistung, A., & Reichenbach, J. R. (2012). Quantitative susceptibility mapping for investigating subtle susceptibility variations in the human brain. *NeuroImage*, *62*(3), 2083–2100.

Smith, A. (1982). *Symbol digit modalities test: Manual*. Los Angeles: Western Psychological Services.

Smith, S. M., Jenkinson, M., Johansen-Berg, H., Rueckert, D., Nichols, T. E., Mackay, C. E., ... Behrens, T. E. (2006). Tract-based spatial statistics: Voxelwise analysis of multi-subject diffusion data. *NeuroImage*, *31*(4), 1487–1505.

Smith, S. M., Zhang, Y., Jenkinson, M., Chen, J., Matthews, P. M., Federico, A., & De Stefano, N. (2002). Accurate, robust, and automated longitudinal and cross-sectional brain change analysis. *NeuroImage*, *17*(1), 479–489.

Tovar-Moll, F., Evangelou, I. E., Chiu, A. W., Richert, N. D., Ostuni, J. L., Ohayon, J. M., ... Bagnato, F. (2009). Thalamic involvement and its impact on clinical disability in patients with multiple sclerosis: A diffusion tensor imaging study at 3T. *American Journal of Neuroradiology*, *30*(7), 1380–1386.

Walsh, A. J., Blevins, G., Lebel, R. M., Seres, P., Emery, D. J., & Wilman, A. H. (2014). Longitudinal MR imaging of iron in multiple sclerosis: An imaging marker of disease. *Radiology*, *270*(1), 186–196.

Westlye, L. T., Walhovd, K. B., Dale, A. M., Bjornerud, A., Due-Tonnessen, P., Engvig, A., ... Fjell, A. M. (2010). Life-span changes of the human brain white matter: Diffusion tensor imaging (DTI) and volumetry. *Cerebral Cortex*, *20*(9), 2055–2068.

Winkler, A. M., Ridgway, G. R., Douaud, G., Nichols, T. E., & Smith, S. M. (2016). Faster permutation inference in brain imaging. *NeuroImage*, *141*, 502–516.

Winkler, A. M., Ridgway, G. R., Webster, M. A., Smith, S. M., & Nichols, T. E. (2014). Permutation inference for the general linear model. *NeuroImage*, *92*, 381–397.

Winkler, A. M., Webster, M. A., Brooks, J. C., Tracey, I., Smith, S. M., & Nichols, T. E. (2016). Non-parametric combination and related permutation tests for neuroimaging. *Human Brain Mapping*, *37*(4), 1486–1511.

Wisnieff, C., Ramanan, S., Olesik, J., Gauthier, S., Wang, Y., & Pitt, D. (2015). Quantitative susceptibility mapping (QSM) of white matter multiple sclerosis lesions: Interpreting positive susceptibility and the presence of iron. *Magnetic Resonance in Medicine*, *74*(2), 564–570.

Wu, B., Li, W., Guidon, A., & Liu, C. (2012). Whole brain susceptibility mapping using compressed sensing. *Magnetic Resonance in Medicine*, *67*(1), 137–147.

Zhang, H., Schneider, T., Wheeler-Kingshott, C. A., & Alexander, D. C. (2012). NODDI: Practical in vivo neurite orientation dispersion and density imaging of the human brain. *NeuroImage*, *61*(4), 1000–1016.

Zhang, J., Tao, R., Liu, C., Wu, W., Zhang, Y., Cui, J., & Wang, J. (2013). Possible effects of iron deposition on the measurement of DTI metrics in deep gray matter nuclei: An in vitro and in vivo study. *Neuroscience Letters*, *551*, 47–52.

Zivadinov, R., Heininen-Brown, M., Schirda, C. V., Poloni, G. U., Bergsland, N., Magnano, C. R., ... Dwyer, M. G. (2012). Abnormal subcortical deep-gray matter susceptibility-weighted imaging filtered phase measurements in patients with multiple sclerosis: A case-control study. *NeuroImage*, *59*(1), 331–339.

How to cite this article: Bergsland N, Schweser F, Dwyer MG, Weinstock-Guttman B, Benedict RH, Zivadinov R. Thalamic white matter in multiple sclerosis: A combined diffusion-tensor imaging and quantitative susceptibility mapping study. *Hum Brain Mapp.* 2018;39:4007–4017. https://doi.org/10.1002/hbm.24227